Mutation of *weak atrium/atrial myosin heavy chain* disrupts atrial function and influences ventricular morphogenesis in zebrafish

Eli Berdougo[1], Hope Coleman[1], Diana H. Lee[1], Didier Y. R. Stainier[2] and Deborah Yelon[1,*]

[1]Developmental Genetics Program and Department of Cell Biology, Skirball Institute of Biomolecular Medicine, New York University School of Medicine, New York, NY 10016, USA
[2]Department of Biochemistry and Biophysics and Programs in Developmental Biology, Genetics, and Human Genetics, University of California, San Francisco, San Francisco, CA 94143, USA
*Author for correspondence (e-mail: yelon@saturn.med.nyu.edu)

Accepted 28 August 2003

Development 130, 6121-6129

doi:10.1242/dev.00838

Summary

The embryonic vertebrate heart is composed of two major chambers, a ventricle and an atrium, each of which has a characteristic size, shape and functional capacity that contributes to efficient circulation. Chamber-specific gene expression programs are likely to regulate key aspects of chamber formation. Here, we demonstrate that epigenetic factors also have a significant influence on chamber morphogenesis. Specifically, we show that an atrium-specific contractility defect has a profound impact on ventricular development. We find that the zebrafish locus *weak atrium* encodes an atrium-specific myosin heavy chain that is required for atrial myofibrillar organization and contraction. Despite their atrial defects, *weak atrium* mutants can maintain circulation through ventricular contraction. However, the *weak atrium* mutant ventricle becomes unusually compact, exhibiting a thickened myocardial wall, a narrow lumen and changes in myocardial gene expression. As *weak atrium/atrial myosin heavy chain* is expressed only in the atrium, the ventricular phenotypes in *weak atrium* mutants represent a secondary response to atrial dysfunction. Thus, not only is cardiac form essential for cardiac function, but there also exists a reciprocal relationship in which function can influence form. These findings are relevant to our understanding of congenital defects in cardiac chamber morphogenesis.

Movies available online

Key words: Zebrafish, Ventricle, Atrium, Cardiac myosin heavy chain, Chamber formation, Atrial natriuretic factor

Introduction

The embryonic vertebrate heart is initially divided into two major chambers, a ventricle and an atrium, each with a characteristic morphology and contractile rhythm (Yelon and Stainier, 1999). Coordinated sequential contractions of the chambers drive circulation unidirectionally from the atrium, to the ventricle, through the vasculature and back to the origin of the circulatory loop. Proper chamber formation is essential for the maintenance of efficient circulation, and congenital heart defects often include abnormal chamber morphologies (Hoffman and Kaplan, 2002). Little is known about the mechanisms that regulate the size and shape of the cardiac chambers.

Intrinsic chamber-specific differentiation pathways clearly play a major role in the acquisition of chamber morphology. For example, in mice, the bHLH transcription factors Hand1 and Hand2 are required for normal ventricular growth and morphology (Firulli et al., 1998; Riley et al., 1998; Riley et al., 2000; Srivastava et al., 1997), and the T-box transcription factor Tbx5 is essential for normal atrial morphogenesis (Bruneau et al., 2001).

In addition to its genetic regulation, chamber morphology may also be susceptible to epigenetic influences. The morphology of the adult heart is known to be responsive to increased functional demand; for example, pressure overload can stimulate ventricular hypertrophy (Seidman and Seidman, 2001). The embryonic heart can also respond to hemodynamic changes; one striking example comes from a recent study in which a physical blockade of blood flow was shown to cause defects in valve formation, bulbus arteriosus formation and cardiac looping in the zebrafish embryo (Hove et al., 2003). Can embryonic hemodynamics also influence the morphology of the ventricle and the atrium – the number of cells in each chamber, the thickness of the chamber wall and the dimensions of the chamber lumen?

To understand the regulation of chamber morphogenesis, we have identified a number of zebrafish mutations that cause cardiac chamber defects (Alexander et al., 1998; Stainier et al., 1996). One of these mutations, *weak atrium* (*wea*), exhibits defects in both chambers: contractility defects in the atrium and morphological defects in the ventricle. Through candidate gene analysis, we demonstrate that *wea* mutations disrupt the zebrafish *atrial myosin heavy chain* (*amhc*) gene. Loss of *amhc* function can explain the atrial contractile defects in *wea* mutants. However, because expression of *amhc* is restricted to the atrium, the *wea* mutant ventricular phenotype, including defects in chamber circumference, wall thickness, lumen size and gene expression, represents a ventricular response to atrial dysfunction. Thus, our studies of *wea* mutants clearly indicate that function of one chamber can influence morphogenesis of

the other, which implicates epigenetic factors in the regulation of chamber morphology.

Materials and methods

Zebrafish

All zebrafish and embryos were maintained at 28°C and staged as previously described (Westerfield, 1995). *wea*^{m58} and *wea*^{sk7} are recessive mutations that segregate in a Mendelian fashion. Homozygous mutant embryos were generated by mating adult heterozygotes. No phenotypes are apparent in *wea* heterozygotes. The *wea*^{sk7} mutation was identified during a screen for ethylnitrosourea-induced mutations that disrupt cardiogenesis in haploids (D.H.L., A. F. Schier and D.Y., unpublished). *wea*^{m58} and *wea*^{sk7} fail to complement each other: in crosses between heterozygotes, 25.3% (53/209) of the progeny exhibit the *wea* mutant phenotype. The *wea*^{m58} and *wea*^{sk7} mutant phenotypes are identical in all characterized aspects; all data shown are from *wea*^{m58} mutants.

Immunofluorescence, in situ hybridization and photography

Whole-mount immunofluorescence experiments were performed as previously described (Yelon et al., 1999), using the monoclonal antibodies MF20 (Bader et al., 1982), S46 (generous gift from F. Stockdale) and CH1 (Lin et al., 1985). MF20 and CH1 were obtained from the Developmental Studies Hybridoma Bank, maintained by the Department of Biological Sciences, University of Iowa, under contract NO1-HD-2-3144 from the NICHD.

In situ hybridization experiments with *vmhc* and *cmlc2* antisense probes were performed as previously described (Yelon et al., 1999). An antisense *amhc* probe was synthesized from a 645 bp fragment of *amhc* cDNA (beginning at nucleotide 2802). An antisense *anf* probe was synthesized from a 422 bp fragment of *anf* cDNA (see below).

Stained embryos were examined with Zeiss Axioplan and M2Bio microscopes, and photographed with a Zeiss Axiocam digital camera. Images were processed using Zeiss Axiovision and Adobe Photoshop software. Live embryo videos were recorded and processed using an Optronics DEI750 video camera and an Axioplan microscope, and Pixelink, QuickTimePro and iMovie software.

Cloning of zebrafish *amhc, vmhc* and *anf* cDNAs

To identify a zebrafish *amhc* gene, we evaluated the expression patterns of available zebrafish ESTs (RZPD, Berlin) resembling myosin heavy chain genes, found one that was atrium-specific (fc52a03) (Clark et al., 2001), and cloned a corresponding full-length cDNA using previously described reverse transcription and RACE techniques (Keegan et al., 2002). To detect *amhc* mutations, we amplified fragments of *amhc* cDNA from mutant embryos using previously described RT-PCR strategies (Keegan et al., 2002). For these experiments, mutant embryos were generated by mating *wea* homozygotes that had survived to adulthood. All sequences were confirmed in at least two independent amplifications of each region of cDNA. Oligonucleotides used for *amhc* amplification were:

5′-CGCTCGCTGATGTCCTCCAGTTCT-3′ with 5′-TCCACCT-GAGCAGACGTGGCTCC-3′;

5′-AGTGTTTACAGTCTTCCCAGCGCCGG-3′ with 5′-CTCCA-ACGTTCCCTTGCTCGAGTCCT-3′; and

5′-AGCCACTACCGCCTCTCTACGG-3′ with 5′-GTTGGAATT-GGACGACCTTGCC-3′.

We also cloned a full-length *vmhc* cDNA, using RACE initiated from our previously reported partial cDNA clone (AF114427) (Yelon et al., 1999). Oligonucleotides used for *vmhc* RACE were: 5′-TT-GCACTGCCTCTTCCACTTCTGTCTG-3′ and 5′-GTTCTTCTTC-ATCCTCTCCAGGTGAGC-3′.

The coding sequences of both *amhc* and *vmhc* appear polymorphic in wild-type zebrafish strains from our fish facility (E.B. and D.Y., unpublished); reported sequences represent the most common wild-type allele.

To identify a zebrafish *anf* gene, we assembled a consensus cDNA sequence from available ESTs (zeh1304, zeh1366, zah4805, zah5977, zeh11098 and bb02c03) and then amplified a 422 bp cDNA fragment using the oligonucleotides 5′-ACACGTTGAGCAGACACAGC-3′ and 5′-TGTTAACAAATTAAGCCGTATTGT-3′.

GenBank Accession Numbers are AY138982 (*amhc*), AY138983 (*vmhc*) and AY319419 (*anf*).

Radiation hybrid mapping and linkage analysis

Physical mapping of *amhc* with a radiation hybrid panel and meiotic mapping of *wea* with SSLP markers were performed using previously described protocols (Keegan et al., 2002; Yelon et al., 2000). Linkage of *amhc* and *wea* was also confirmed by demonstrating that the *wea*^{m58} mutant phenotype and the single-base deletion detected in *wea*^{m58} mutants are tightly linked (0 recombinants in 188 meioses). Additional radiation hybrid mapping placed *vmhc* on LG2 near Z8517.

Morpholino microinjection

Wild-type embryos were injected at the one-cell or two-cell stage with 1-3 ng of anti-*amhc* morpholino (GeneTools). The anti-*amhc* morpholino (5′-ACTCTGCCATTAAAGCATCACCCAT-3′) is predicted to block translation of Amhc.

Transmission electron microscopy

Embryos were fixed at 48 hours postfertilization (hpf) with 2% paraformaldehyde and 2.5% glutaraldehyde in 0.1 M sodium cacodylate buffer, postfixed with 1% osmium tetraoxide followed by 1% uranyl acetate, dehydrated through a graded series of ethanol washes, and embedded in LX112 resin (LADD Research Industries, Burlington, VT). Ultrathin (80 nm) sections were cut on a Reichert Ultracut UCT, stained with uranyl acetate followed by lead citrate, and viewed on a JEOL 1200EX transmission electron microscope at 80 kV.

Histology

Prior to sectioning, embryos were fixed in 4% paraformaldehyde, dehydrated through an ethanol series, cleared in xylene and embedded in paraffin wax. 4 μm longitudinal sections were cut, dewaxed, dried, and stained with Hematoxylin and Eosin.

Results

The *weak atrium* locus is required for atrial contractility

Mutation of the zebrafish *weak atrium* (*wea*) locus causes atrial contractility defects that are easily observed in live embryos (see Movie 1 at http://dev.biologists.org/supplemental/). In wild-type embryos, the atrium exhibits vigorous, rhythmic contractions; in *wea* mutant embryos, the atrial walls remain relatively still. This atrial defect is apparent from the time of initiation of the embryonic heartbeat and, over time, the atrial chamber becomes dilated (Fig. 1A,B). In contrast to the atrium, the *wea* mutant ventricle contracts at a normal rate [see Movie 1 at http://dev.biologists.org/supplemental/; at 48 hours hpf, wild-type ventricles contracted at 139±22 beats/min (n=5) and *wea* ventricles contracted at 150±26 beats/min (n=10)].

Despite the lack of an atrial pump, circulation proceeds through the heart and vasculature of *wea* mutants (see Movie 1 at http://dev.biologists.org/supplemental/). However, a characteristic blood pool caudal to the *wea* mutant atrium indicates that blood flow is inefficient relative to wild type

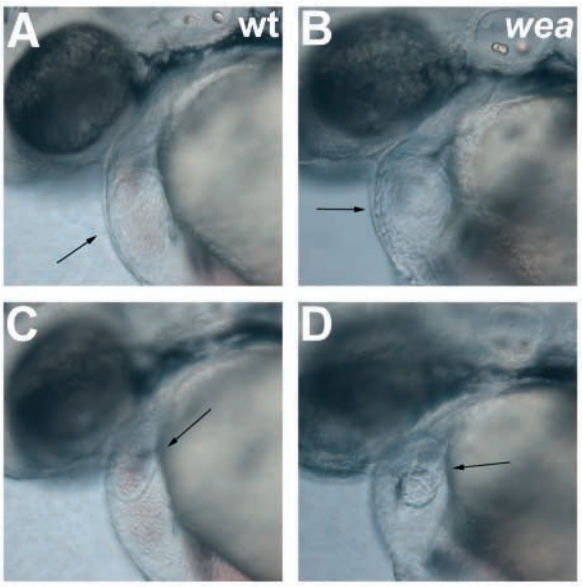

Fig. 1. Cardiac morphology in *wea* mutant embryos. (A-D) Lateral views of live embryos at 48 hpf, anterior to the left. (A,B) Atrial plane of focus. Compared with the wild-type (wt) atrium (A, arrow), the *wea* mutant atrium (B, arrow) appears dilated. (C,D) Ventricular plane of focus. Compared with the wild-type ventricle (C, arrow), the *wea* mutant ventricle (D, arrow) appears slightly compact. Mutant embryos shown are wea^{m58} homozygotes. The wea^{m58} and wea^{sk7} mutant phenotypes are identical in all characterized aspects; data in all figures are from wea^{m58} mutants.

(see Movie 1 at http://dev.biologists.org/supplemental/). Nevertheless, *wea* mutants do not exhibit any general growth defects or obvious abnormalities in organs other than the heart (data not shown) (Chen et al., 1996; Stainier et al., 1996). In fact, some homozygous *wea* mutants can survive to become fertile adults. In *wea* mutant survivors, ventricular function continues and valve and vessel formation proceed; however, atrial defects remain throughout life (E.B. and D.Y., unpublished). Multiple *wea* alleles with these phenotypic characteristics have been identified in screens focused on mutations disrupting cardiac form and function (Alexander et al., 1998; Chen et al., 1996; Stainier et al., 1996). Here, we focus on two *wea* alleles: wea^{m58} (Stainier et al., 1996) and wea^{sk7} (see Materials and methods).

wea is required for assembly of the atrial contractile apparatus

The functional defects in *wea* mutants suggest that the atrial contractile apparatus is abnormal. We compared sarcomere assembly in wild-type and *wea* mutant embryos at 48 hpf. At this stage, the wild-type atrium exhibits nascent sarcomeres containing both thick and thin filaments (Fig. 2A) (Wanga et al., 2001). By contrast, the *wea* mutant atrium lacks organized myofibrillar arrays: some mutant atrial cells contain no obvious myofilaments (data not shown), whereas others contain a small number of poorly organized myofilaments (Fig. 2B, arrow). Ventricular sarcomere assembly is intact in both wild-type and *wea* mutant embryos (Fig. 2C,D). These data suggest that *wea* encodes an atrium-specific component of the sarcomere.

wea mutations disrupt expression of *atrial myosin heavy chain*

Using whole-mount immunofluorescence, we examined the status of sarcomere proteins in the *wea* mutant heart. The monoclonal antibody S46 recognizes an atrium-specific sarcomeric myosin heavy chain epitope in zebrafish (Stainier and Fishman, 1992). *wea* mutants do not exhibit detectable S46 staining at any stage (Fig. 3A,B, and data not shown). Additionally, the monoclonal antibody MF20, which recognizes a sarcomeric myosin heavy chain epitope found in both the ventricle and atrium (Stainier and Fishman, 1992), fails to stain the *wea* atrium, but stains the *wea* ventricle normally (Fig. 3A,B). These results suggest that the *wea* mutant atrium lacks myosin heavy chain proteins. Other sarcomere proteins, including tropomyosin, α-actin and cardiac troponin T, appear present at normal levels throughout the *wea* heart (Fig. 3C,D, and data not shown).

For further examination of atrial myosin heavy chain expression in *wea* mutants, we cloned a zebrafish *atrial myosin heavy chain* (*amhc*) gene (see Materials and methods). The zebrafish *amhc* gene contains a 5810 bp open reading frame (orf) that is 74% identical to the nucleotide sequence of the orf of the zebrafish *ventricular myosin heavy chain* (*vmhc*) gene. Comparing protein sequences, zebrafish Amhc is 83% identical to zebrafish Vmhc, and 86% identical to mouse cardiac myosin heavy chains, indicating that cardiac myosin heavy chain structure is well conserved.

In wild-type embryos, *amhc* expression begins around the 19-somite stage, slightly later than the initiation of *vmhc*

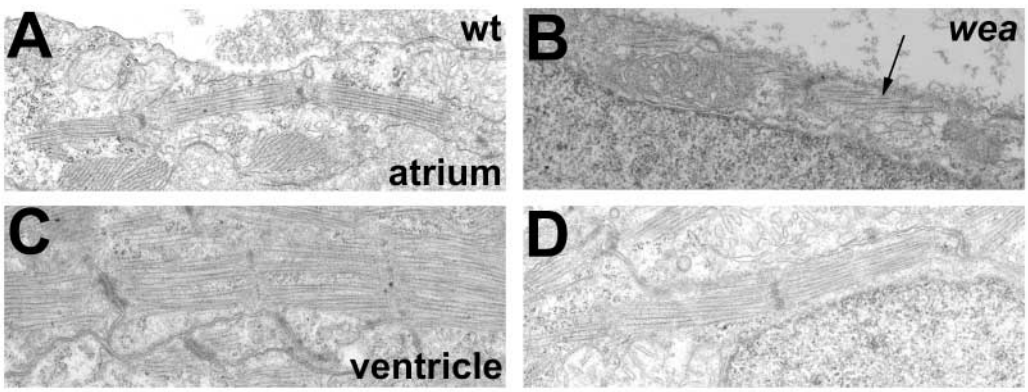

Fig. 2. Myocardial ultrastructure is disrupted in the *wea* mutant atrium and intact in the *wea* mutant ventricle. (A-D) Longitudinal sections of myocardiocytes at 48 hpf viewed by transmission electron microscopy. (A,B) Atrial cells in wild-type embryos contain myofibrillar arrays (A), but myofibrils are rarely found in *wea* mutant atrial cells (B). Occasionally, *wea* mutant atrial cells contain a few disorganized myofilaments (B, arrow). (C,D) Ventricular cells in wild-type (C) and *wea* mutant embryos (D) contain normal myofibrillar arrays.

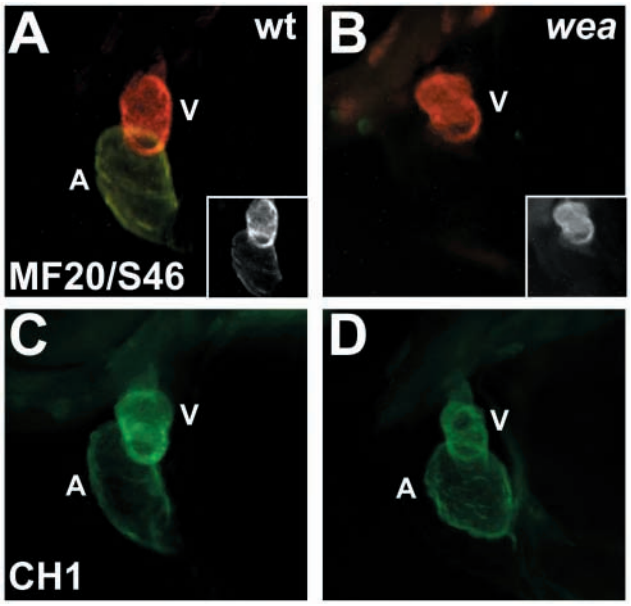

Fig. 3. The *wea* mutant atrium lacks atrial myosin heavy chain. (A-D) Lateral views at 48 hpf, anterior to the left. (A,B) Whole-mount immunofluorescence with MF20 (TRITC) and S46 (FITC). In wild-type embryos (A), double exposure indicates MF20 staining in the ventricle (red), and overlap of MF20 and S46 staining in the atrium (yellow). Ventricle (V) and atrium (A) are indicated. Inset shows MF20 staining only; immunoreactivity in both chambers is clear. In *wea* mutant embryos (B), double exposure indicates that MF20 stains the ventricle (red), but neither MF20 nor S46 stain the atrium. Inset, showing MF20 alone, reinforces that MF20 stains only the ventricle in *wea* mutants. (C,D) Whole-mount immunofluorescence with the anti-tropomyosin antibody CH1 (FITC). CH1 stains both chambers in wild-type (C) and *wea* mutant embryos (D). Note that the *wea* mutant ventricle appears smaller than the wild-type ventricle.

expression, which begins around the 13-somite stage (Yelon et al., 1999). From its onset, *amhc* expression is complementary to *vmhc* expression: the expression patterns of *vmhc* and *amhc* subdivide the myocardial precursors into two separate populations that are likely to represent the ventricular and atrial precursors (Fig. 4) (Yelon et al., 1999). For example, at the 21-somite stage, the inner portion of the cardiac myosin light chain 2 (*cmlc2*; *mylc2a* – Zebrafish Information Network)-expressing myocardial cone expresses *vmhc*, and the outer portion expresses *amhc* (Fig. 4A-C). The cardiac cone then elongates to form a heart tube with *vmhc*-expressing cells at one end and *amhc*-expressing cells at the other (Fig. 4E-G). By 48 hpf, the *vmhc*-expressing ventricle and *amhc*-expressing atrium are morphologically distinct within the looped heart (Fig. 4I-K). We have never observed *amhc* expression in the ventricle, nor have we observed *vmhc* expression in the atrium.

Neither *wea*^{m58} nor *wea*^{sk7} mutants exhibit robust expression of *amhc* (Fig. 4D,H,L, and data not shown). Initial *amhc* expression is detectable in *wea* mutants (Fig. 4D), but there is no evident expression at later stages (Fig. 4H,L). By contrast, other cardiac genes, such as *cmlc2*, *cmlc1*, *vmhc*, *nkx2.5*, *tbx20* and *tbx5*, are expressed at normal levels in the *wea* mutant heart (stages examined range from 24-48 hpf, data not shown).

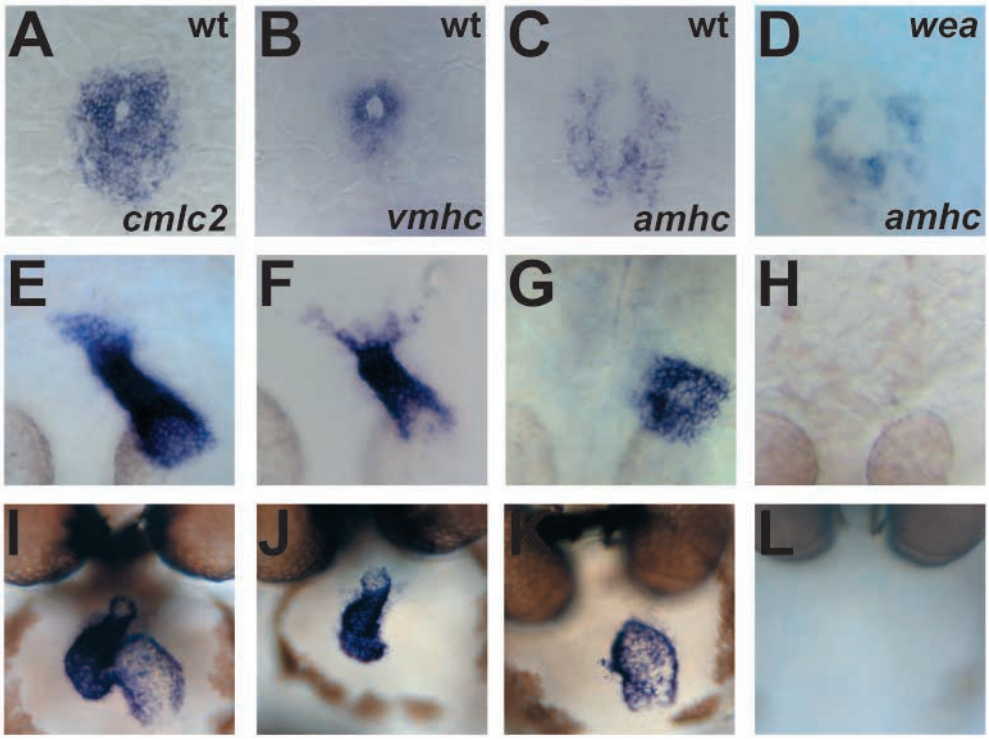

Fig. 4. *amhc* is expressed only in atrial myocardium. (A-L) Whole-mount in situ hybridization compares expression of *cmlc2* (A,E,I), *vmhc* (B,F,J) and *amhc* (C,D,G,H,K,L). (A-D) Dorsal views at the 21-somite stage, anterior to the top. In wild-type embryos (A-C), *cmlc2* expression (A) is observed throughout the cardiac cone. Presumed ventricular precursors express *vmhc* (B) and are found in the central portion of the cardiac cone. At this stage, presumed atrial precursors are beginning to express *amhc* (C) and are found in the outer portion of the cardiac cone. (E-H) Dorsal views through the head at 24 hpf, anterior to the bottom. In wild-type embryos (E-G), *cmlc2* (E) is expressed throughout the heart tube, *vmhc* (F) is expressed in the ventricular precursors, and *amhc* (G) is expressed in the atrial precursors. (I-L) Frontal views at 48 hpf, head to the top. In wild-type embryos, *cmlc2* (I) is expressed throughout the heart, *vmhc* (J) is expressed in the ventricle, and *amhc* (K) is expressed in the atrium. *wea* mutant embryos express *amhc* in atrial precursors initially (D), but do not maintain *amhc* expression (H,L). At all stages examined, ranging from the 19-somite stage through adulthood, there appears to be little, if any, overlap between *vmhc* and *amhc* expression. We have not observed *amhc* expression anywhere outside of the atrium.

The *wea* locus encodes Amhc

Hypothesizing that *wea* could encode Amhc or a regulator of *amhc* expression, we chose to map both *amhc* and *wea*. Using radiation hybrid panels (Geisler et al., 1999; Hukriede et al., 2001), we mapped *amhc* to zebrafish LG20 near the SSLP marker Z4329 (Shimoda et al., 1999). Through meiotic mapping, we mapped *wea* to the same region of LG20 (near Z7568). The concordance of these map positions made *amhc* a strong candidate gene for the *wea* locus.

We proceeded to look for *amhc* mutations in cDNA isolated from wea^{m58} and wea^{sk7} mutants. cDNA from wea^{m58} mutants has a deletion of a single T at position 4024 of the *amhc* orf (Fig. 5A), creating a frame-shift that would produce 66 missense codons followed by a stop codon. cDNA from wea^{sk7} mutants contains a T to A substitution at position 4577 of the *amhc* orf, creating a stop codon (Fig. 5B). The premature stop codons found in both wea^{m58} and wea^{sk7} suggest that the decreased stability of the mutant *amhc* RNA (Fig. 4H,L) could be the result of nonsense-mediated decay (Culbertson, 1999; Hentze and Kulozik, 1999). Based on the lack of MF20 and S46 immunoreactivity (Fig. 3B), and the low levels of *amhc* RNA (Fig. 4H,L), in the *wea* mutant atrium, it is unlikely that *wea* mutants contain much Amhc protein. Even so, both mutant *amhc* cDNAs would be predicted to encode truncated Amhc proteins that, if stable, could be deficient in dimerization and/or aggregation (Fig. 5C). Together, our data suggest that wea^{m58} and wea^{sk7} are strong hypomorphic, if not null, alleles of *amhc*.

To confirm that *wea* mutations cause a strong loss-of-function of *amhc*, we compared the phenotypes of *wea* mutant embryos and embryos injected with an antisense morpholino (Nasevicius and Ekker, 2000; Summerton and Weller, 1997) designed to inhibit Amhc translation. Injection of the anti-*amhc* morpholino phenocopies the *wea* mutation (Fig. 5D-F). Morpholino-injected embryos lack atrial contractility and do not display S46 or MF20 atrial immunoreactivity. Together, our analyses of S46 immunoreactivity, *amhc* expression, genetic linkage, *amhc* mutations and an anti-*amhc* morpholino indicate that *wea* encodes Amhc.

Ventricular morphology responds to atrial dysfunction

As myosin heavy chains are essential for myofibrillogenesis, the lack of functional Amhc in *wea* mutants can account for the observed defects in atrial myofibrillar organization and contractility. In addition to their atrial defects, *wea* mutants exhibit significant ventricular defects. As *amhc* expression is restricted to the atrium (Fig. 4), any ventricular phenotypes in *wea* mutants are likely to represent secondary consequences of atrial dysfunction.

During the first 36 hours of development, ventricular form and function appear normal in *wea* mutants (Fig. 6A-C, and data not shown). By 48 hpf, although the rhythm of ventricular contractions remains normal, the *wea* mutant ventricle acquires an unusual and variable morphology (Fig. 6D-F; also see Movie 1 at http://dev.biologists.org/supplemental/, Fig. 1C,D, Fig. 3 and Fig. 5D-F). Specifically, the *wea* mutant ventricle becomes more compact, with a smaller circumference than the wild-type ventricle. Sections through the *wea* mutant heart reveal significant thickening of the ventricular wall and narrowing of the ventricular lumen (Fig. 7). The thickness of the *wea* ventricular wall varies between, and within, individual embryos, which is in contrast to the consistent and uniform structure of the wild-type ventricular wall (Fig. 7C,D). Increased ventricular thickness in *wea* mutants does not seem to be caused by excess proliferation. The number of ventricular myocardial cells varies between *wea* mutant embryos, but is

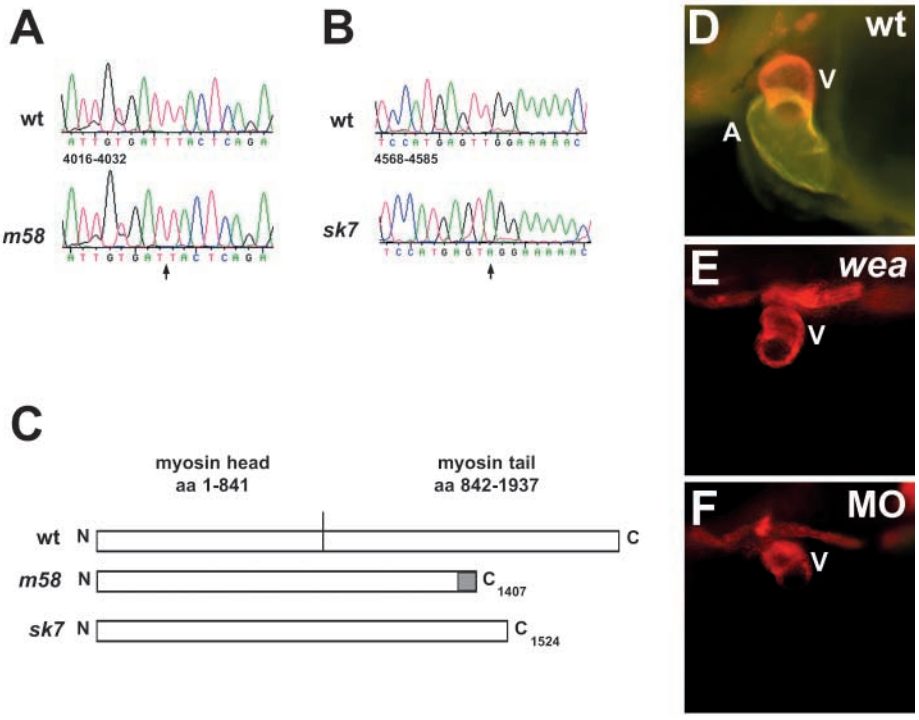

Fig. 5. wea^{m58} and wea^{sk7} are strong loss-of-function alleles of *amhc*. (A) The wea^{m58} mutation is a deletion of a single T at position 4024 of the *amhc* orf, which creates a frame-shift (arrow points to the position of the missing T). (B) The wea^{sk7} mutation is a T to A substitution at position 4577 of the *amhc* orf, which creates a premature stop codon (arrow points to the mutation). (C) Both mutant *amhc* cDNAs are predicted to encode truncated Amhc proteins. The wild-type Amhc protein contains 1937 amino acids, the predicted wea^{m58} Amhc protein would contain 66 missense amino acids (gray bar) and would terminate after amino acid 1407, and the predicted wea^{sk7} Amhc protein would terminate after amino acid 1524. (D-F) Lateral views at 48 hpf, anterior to the left, of whole-mount immunofluorescence with MF20 (TRITC) and S46 (FITC). Ventricle (V) and atrium (A) are indicated. Phenotype of wild-type (D) and *wea* mutant embryos (E) is as described in Fig. 3. Embryos injected with an anti-*amhc* morpholino (F) exhibit a phenotype indistinguishable from that of *wea* mutant embryos (E). 138/138 morpholino-injected embryos phenocopy the *wea* mutation, and 120/120 embryos injected with a control morpholino appear wild type. Note that the *wea* mutant ventricle (E) and the morpholino-injected ventricle (F) both appear smaller than the wild-type ventricle (D).

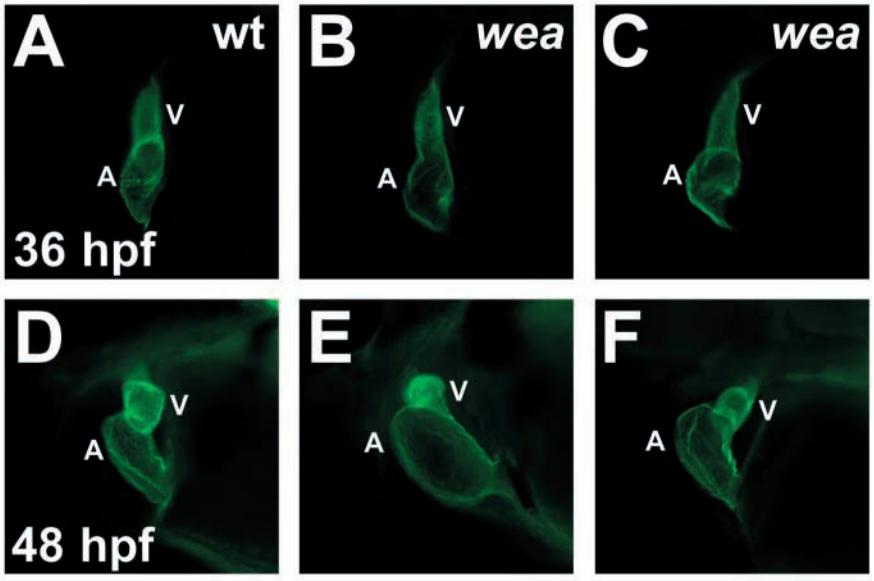

Fig. 6. Defects in ventricular morphology emerge by 48 hpf in *wea* mutants. (A-F) Lateral views, anterior to the left, of whole-mount immunofluorescence with the anti-tropomyosin antibody CH1 (FITC). Ventricle (V) and atrium (A) are indicated. (A-C) At 36 hpf, the wild-type ventricle (A) and the *wea* mutant ventricle (B,C) have similar morphology. The *wea* mutant atrium is slightly dilated at this stage. (D-F) At 48 hpf, the *wea* mutant ventricle (E,F) is noticeably smaller than the wild-type ventricle (D). The morphology of the *wea* mutant ventricle varies between individuals (E,F), as does the degree of dilation of the *wea* mutant atrium. Distortion of cardiac looping is also apparent in *wea* mutants at this stage.

not greater than the number found in wild-type embryos [at 72 hpf, the total number of ventricular myocardial nuclei in serial sections from wild-type embryos was 350±15 (n=2) compared with 274±70 (n=3) in sections from *wea* mutant embryos]. All characterized features of the *wea* ventricular phenotype are found in both wea^{m58} and wea^{sk7} mutants, and in embryos injected with the anti-*amhc* morpholino. Overall, the *wea* ventricular phenotype indicates that a loss of atrial function indirectly stimulates reorganization of the ventricular myocardium, producing significant changes in ventricular form.

Myocardial gene expression responds to atrial dysfunction

Changes in ventricular morphology are likely to be accompanied by changes in myocardial gene expression. In particular, we expected that the ventricular response in *wea* mutants could involve gene expression changes similar to those observed in mammalian cardiomyopathies. To confirm this, we chose to examine the *atrial natriuretic factor* (*anf*) gene because of its established responsiveness to a variety of physiological stimuli, including conditions causing hypertrophic or dilated cardiomyopathy in mammals (e.g. Aronow et al., 2001; Barrans et al., 2002; Hwang et al., 2002; Cameron and Ellmers, 2003). We also assessed expression of the *cmlc2* gene (Yelon et al., 1999), as genes encoding sarcomere components are often upregulated in response to pathologic conditions (e.g. Aronow et al., 2001; Barrans et al., 2002; Hwang et al., 2002).

As in other species (Zeller et al., 1987; Small and Krieg, 2000; Houweling et al., 2002), the zebrafish *anf* gene is expressed in both the ventricle and atrium before becoming restricted to the atrium (Fig. 8A, and data not shown). In comparison with wild-type embryos, *wea* mutants exhibit striking upregulation of *anf* in both chambers (Fig. 8A,B).

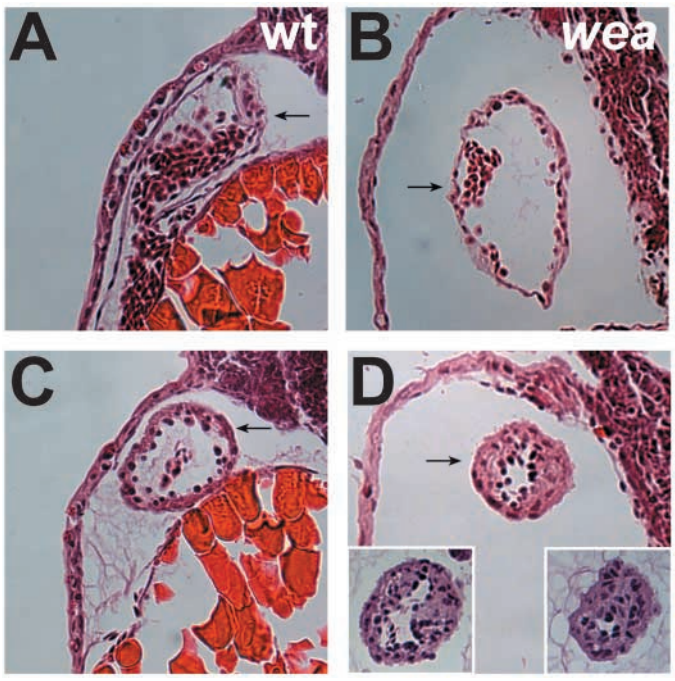

Fig. 7. Ventricular morphology responds to atrial dysfunction in *wea* mutants. (A-D) Longitudinal sections through the heart at 72 hpf, stained with Hematoxylin and Eosin, anterior to the top. (A,B) Sections through the wild-type (A, arrow) and *wea* mutant atrium (B, arrow) demonstrate similar thickness of the atrial wall. The *wea* mutant atrium is dilated in comparison with the wild-type atrium and contains less blood. (C,D) Comparison of sections through the wild-type (C, arrow) and *wea* mutant ventricle (D, arrow) demonstrates that the ventricular wall is thicker, and that the ventricular lumen is narrower, in *wea* mutants. The morphology of the *wea* mutant ventricle varies between individuals (D); insets show two additional examples of ventricular sections from other *wea* mutant embryos. Variability is also apparent within individual embryos, as the *wea* mutant ventricular wall does not exhibit a uniform thickness. (D) Thickening of the *wea* mutant ventricular wall is apparent by 48 hpf, and increases between 48 and 72 hpf (data not shown). All sections shown are the central section from serial sectioning through the respective chamber; results are representative of the examination of more than 15 embryos of each genotype.

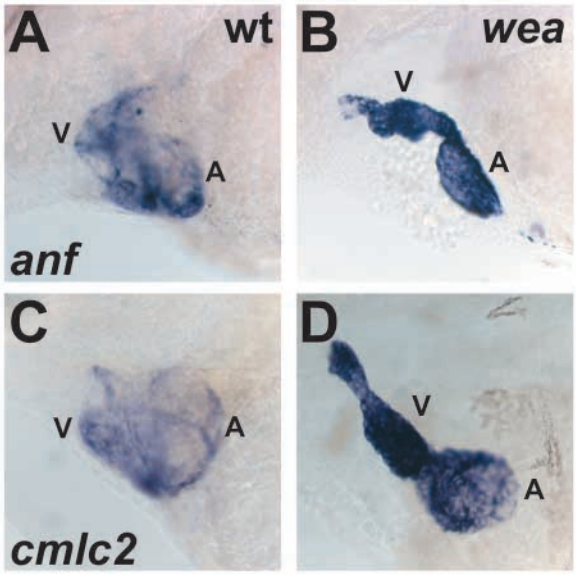

Fig. 8. Myocardial gene expression responds to atrial dysfunction in *wea* mutants. (A-D) Lateral views at 96 hpf, anterior to the left. Whole-mount in situ hybridization compares expression of *anf* (A,B) and *cmlc2* (C,D). Ventricle (V) and atrium (A) are indicated. Embryos were treated with 0.003% phenylthiourea from 24-96 hpf to inhibit pigmentation (Elsalini and Rohr, 2003). Embryos were sorted by phenotype prior to fixing, and tails were marked to distinguish between wild-type and *wea* mutant embryos. Mutant and wild-type siblings were then kept together throughout the in situ protocol, and were stained for the same length of time. (A,B) Comparison of wild-type (A) and *wea* mutant embryos (B) indicates substantial upregulation of *anf* expression throughout the *wea* mutant heart. (C,D) Likewise, the *wea* mutant heart exhibits upregulation of *cmlc2* expression at this stage. Intensity of *anf* and *cmlc2* expression is increased on a per cell basis; this is especially clear for the atrium, which is the same thickness in wild-type and *wea* mutant embryos.

Similarly, *cmlc2* is expressed in both chambers in wild-type embryos and is significantly upregulated throughout the *wea* mutant heart (Fig. 8C,D). Thus, the response to cardiac dysfunction in *wea* mutants shares molecular characteristics with mammalian cardiomyopathies.

Discussion

wea/amhc is essential for atrial function

Chamber-specific components of the contractile apparatus contribute to the distinct functional attributes of the embryonic ventricle and atrium. In the zebrafish embryo, loss-of-function of the atrium-specific gene *amhc* debilitates atrial contractility without affecting ventricular contractions. Without functional Amhc, atrial MF20 immunoreactivity is lost and atrial sarcomere assembly is disrupted. These phenotypes strongly suggest that *amhc* is the major, or only, sarcomeric myosin heavy chain gene expressed in the embryonic zebrafish atrium.

Although the *wea* mutant atrium lacks contractile force, it retains passive function throughout the life of *wea* mutants, serving as a passageway for blood headed into the ventricle. Thus, *wea* mutants provide an opportunity to evaluate the secondary consequences of a loss of atrial function.

Atrial function influences ventricular development

Although intrinsic gene expression programs dictate aspects of cardiac chamber formation, our data indicate that cardiac chambers can also respond to epigenetic influences during their development. Specifically, the changes in shape, size, organization and gene expression of the *wea* mutant ventricle indicate that the ventricular myocardium can respond to atrial failure. In order to conclude that ventricular aspects of the *wea* mutant phenotype are secondary to the loss of *amhc* function, it is essential to establish that *amhc* is not expressed in the ventricle. Although it is difficult to address precisely whether there is overlap of *amhc* and *vmhc* expression at the atrioventricular boundary, it is clear that there are two separate zones of *amhc* and *vmhc* expression that are compatible with the expected locations of atrial and ventricular myocardiocytes throughout development (Yelon et al., 1999).

Although atrial contractility is aberrant in *wea* mutants from the initiation of the embryonic heartbeat (around 24 hpf), the *wea* mutant ventricular defects first become apparent around 48 hpf. This sequence of events fits a model in which the ventricular myocardium responds to a physiological stimulus that is the result of atrial dysfunction. There are several possibilities for the nature of the signal received by the *wea* mutant ventricle. For example, ventricular mechanosensation of hemodynamic changes produced by atrial failure could trigger changes in ventricular morphology and gene expression. Alternatively, oxygen sensors could provide feedback to the ventricle regarding inefficient circulation, or the nonfunctional atrial myocardium could emit stress signals that are perceived by the ventricle.

A comparison of *wea* mutants with other zebrafish mutants with sarcomere defects yields insights regarding potential triggers of the *wea* ventricular phenotype. The zebrafish *silent heart/tnnt2* (*sih*) locus encodes cardiac troponin T (Sehnert et al., 2002), and the *pickwick/ttn* (*pik*) locus encodes titin (Xu et al., 2002). In *sih* and *pik* mutants, neither the atrium nor the ventricle contract or assemble sarcomeres normally (Sehnert et al., 2002; Xu et al., 2002). Additionally, neither the *sih* ventricle nor the *pik* ventricle acquire the compact and thick morphology typical of the *wea* ventricle (Sehnert et al., 2002; Xu et al., 2002). Indeed, *pik* mutants feature a contrasting phenotype, a dilated cardiomyopathy in which the embryonic ventricle becomes unusually thin (Xu et al., 2002). We have also examined the roles of two other zebrafish loci, both of which are required for ventricular sarcomere formation and are dispensable for atrial sarcomere formation (H.C., C. Fabricant and D.Y., unpublished). Like *sih* and *pik*, neither of these ventricular mutants exhibit ventricular thickening. These comparisons indicate that reduced blood flow is not necessarily sufficient to provoke the ventricular phenotypes observed in *wea* mutants. Perhaps a specific type of hemodynamic alteration elicits the *wea* ventricular response, and this physiological circumstance is not replicated when the ventricle, or the entire heart, fails to contract. Alternatively, ventricular contractility and/or sarcomere assembly might provide a degree of cellular integrity that is a prerequisite for the type of chamber morphogenesis observed in *wea* mutants.

Conservation of chamber responsiveness and relevance to congenital heart disease

Zebrafish *wea* mutants demonstrate that epigenetic

parameters can play key roles in regulating ventricular morphogenesis. A recent study suggests that the relationship between atrial function and ventricular development may be conserved among vertebrate species. Specifically, analysis of mice lacking *MLC2a*, an atrial regulatory myosin light chain gene essential for atrial myofibrillogenesis, indicates that loss of atrial function affects ventricular morphology in the mouse embryo (Huang et al., 2003). The conserved influence of function on form is likely to be relevant to the causes of congenital abnormalities in cardiac chamber formation.

When considering the relationship of zebrafish *wea* mutations with human disease, it is important to note that autosomal dominant mutations in human cardiac myosin heavy chain genes can cause either hypertrophic or dilated cardiomyopathy, depending on the specific gene, mutation and individual (Seidman and Seidman, 2001). In affected individuals, missense mutations are thought to be responsible for the production of malfunctional myosin heavy chain proteins that act cell-autonomously to evoke cardiomyopathy. By contrast, loss-of-function *wea* mutations appear entirely recessive, as heterozygotes are phenotypically wild-type. Thus, *wea* mutants demonstrate an alternate method by which a sarcomere defect can trigger a morphogenetic response – not only by directly affecting the cells expressing the mutant gene, but also by indirectly affecting another chamber.

Alterations in circulation, as observed in *wea* mutants, can trigger significant changes in chamber size, shape, cellular organization and gene expression. Our data suggest that similar scenarios could be responsible for congenital heart defects. For example, our studies lend credence to the proposal that hypoplastic left heart syndrome, which includes defects in left ventricular morphogenesis, can be caused by reduced blood flow through the left ventricle (Harh et al., 1973; Grossfeld, 1999; Sedmera et al., 1999; Sedmera et al., 2002). Just as reduced ventricular loading, caused by mitral atresia, is suggested to trigger hypoplastic left heart syndrome (Grossfeld, 1999), reduced ventricular loading in *wea* mutants, caused by atrial failure, is associated with changes in ventricular morphology. Altogether, because of their striking ventricular phenotypes and relevance to congenital heart defects, zebrafish *wea* mutants provide a valuable genetic model for the analysis of the epigenetic mechanisms that influence cardiac chamber formation.

We thank L. Cummins and F. Macaluso of the Albert Einstein College of Medicine Analytical Imaging Facility for expert technical assistance with electron microscopy. We are also grateful to J. Chen for sharing data prior to publication; S. Zimmerman, T. Bruno and N. Dillon for exceptional fish care; A. F. Schier for valuable discussions; and members of the Yelon and Schier labs for advice and support. D.H.L. is supported by the MSTP of the NYU School of Medicine, and the haploid screen was supported by NIH R01 GM64327 granted to A. F. Schier. This work was supported by a Burroughs Wellcome Fund Career Award to D.Y.

References

Alexander, J., Stainier, D. Y. and Yelon, D. (1998). Screening mosaic F1 females for mutations affecting zebrafish heart induction and patterning. *Dev. Genet.* **22**, 288-299.

Aronow, B. J., Toyokawa, T., Canning, A., Haghighi, K., Delling, U., Kranias, E., Molkentin, J. D. and Dorn, G. W., 2nd (2001). Divergent transcriptional responses to independent genetic causes of cardiac hypertrophy. *Physiol. Genomics* **6**, 19-28.

Bader, D., Masaki, T. and Fischman, D. A. (1982). Immunochemical analysis of myosin heavy chain during avian myogenesis in vivo and in vitro. *J. Cell Biol.* **95**, 763-770.

Barrans, J. D., Allen, P. D., Stamatiou, D., Dzau, V. J. and Liew, C. C. (2002). Global gene expression profiling of end-stage dilated cardiomyopathy using a human cardiovascular-based cDNA microarray. *Am. J. Pathol.* **160**, 2035-2043.

Bruneau, B. G., Nemer, G., Schmitt, J. P., Charron, F., Robitaille, L., Caron, S., Conner, D. A., Gessler, M., Nemer, M., Seidman, C. E. et al. (2001). A murine model of Holt-Oram syndrome defines roles of the T-box transcription factor Tbx5 in cardiogenesis and disease. *Cell* **106**, 709-721.

Cameron, V. A. and Ellmers, L. J. (2003). Minireview: natriuretic peptides during development of the fetal heart and circulation. *Endocrinology* **144**, 2191-2194.

Chen, J.-N., Haffter, P., Odenthal, J., Vogelsang, E., Brand, M., van Eeden, F. J., Furutani-Seiki, M., Granato, M., Hammerschmidt, M., Heisenberg, C. P. et al. (1996). Mutations affecting the cardiovascular system and other internal organs in zebrafish. *Development* **123**, 293-302.

Clark, M. D., Hennig, S., Herwig, R., Clifton, S. W., Marra, M. A., Lehrach, H., Johnson, S. L. and the WU-GSC EST Group. (2001). An oligonucleotide fingerprint normalized and expressed sequence tag characterized zebrafish cDNA library. *Genome Res.* **11**, 1594-1602.

Culbertson, M. R. (1999). RNA surveillance. Unforeseen consequences for gene expression, inherited genetic disorders and cancer. *Trends Genet.* **15**, 74-80.

Elsalini, O. A. and Rohr, K. B. (2003). Phenylthiourea disrupts thyroid function in developing zebrafish. *Dev. Genes Evol.* **212**, 593-598.

Firulli, A. B., McFadden, D. G., Lin, Q., Srivastava, D. and Olson, E. N. (1998). Heart and extra-embryonic mesodermal defects in mouse embryos lacking the bHLH transcription factor Hand1. *Nat. Genet.* **18**, 266-270.

Geisler, R., Rauch, G. J., Baier, H., van Bebber, F., Brobeta, L., Dekens, M. P., Finger, K., Fricke, C., Gates, M. A., Geiger, H. et al. (1999). A radiation hybrid map of the zebrafish genome. *Nat. Genet.* **23**, 86-89.

Grossfeld, P. D. (1999). The genetics of hypoplastic left heart syndrome. *Cardiol. Young* **9**, 627-632.

Harh, J. Y., Paul, M. H., Gallen, W. J., Friedberg, D. Z. and Kaplan, S. (1973). Experimental production of hypoplastic left heart syndrome in the chick embryo. *Am. J. Cardiol.* **31**, 51-56.

Hentze, M. W. and Kulozik, A. E. (1999). A perfect message: RNA surveillance and nonsense-mediated decay. *Cell* **96**, 307-310.

Hoffman, J. I. and Kaplan, S. (2002). The incidence of congenital heart disease. *J. Am. Coll. Cardiol.* **39**, 1890-1900.

Houweling, A. C., Somi, S., Van Den Hoff, M. J., Moorman, A. F. and Christoffels, V. M. (2002). Developmental pattern of ANF gene expression reveals a strict localization of cardiac chamber formation in chicken. *Anat. Rec.* **266**, 93-102.

Hove, J. R., Koster, R. W., Forouhar, A. S., Acevedo-Bolton, G., Fraser, S. E. and Gharib, M. (2003). Intracardiac fluid forces are an essential epigenetic factor for embryonic cardiogenesis. *Nature* **421**, 172-177.

Huang, C., Sheikh, F., Hollander, M., Cai, C., Becker, D., Chu, P.-H., Evans, S. and Chen, J. (2003). Embryonic atrial function is essential for mouse embryogenesis, cardiac morphogenesis and angiogenesis. *Development* **130**, 6111-6119.

Hukriede, N., Fisher, D., Epstein, J., Joly, L., Tellis, P., Zhou, Y., Barbazuk, B., Cox, K., Fenton-Noriega, L., Hersey, C. et al. (2001). The LN54 radiation hybrid map of zebrafish expressed sequences. *Genome Res.* **11**, 2127-2132.

Hwang, J. J., Allen, P. D., Tseng, G. C., Lam, C. W., Fananapazir, L., Dzau, V. J. and Liew, C. C. (2002). Microarray gene expression profiles in dilated and hypertrophic cardiomyopathic end-stage heart failure. *Physiol. Genomics* **10**, 31-44.

Keegan, B. R., Feldman, J. L., Lee, D. H., Koos, D. S., Ho, R. K., Stainier, D. Y. R. and Yelon, D. (2002). The elongation factors Pandora/Spt6 and Foggy/Spt5 promote transcription in the zebrafish embryo. *Development* **129**, 1623-1632.

Lin, J. J., Chou, C. S. and Lin, J. L. (1985). Monoclonal antibodies against chicken tropomyosin isoforms: production, characterization, and application. *Hybridoma* **4**, 223-242.

Nasevicius, A. and Ekker, S. C. (2000). Effective targeted gene 'knockdown' in zebrafish. *Nat. Genet.* **26**, 216-220.

Riley, P., Anson-Cartwright, L. and Cross, J. C. (1998). The Hand1 bHLH

transcription factor is essential for placentation and cardiac morphogenesis. *Nat. Genet.* **18**, 271-275.

Riley, P. R., Gertsenstein, M., Dawson, K. and Cross, J. C. (2000). Early exclusion of hand1-deficient cells from distinct regions of the left ventricular myocardium in chimeric mouse embryos. *Dev. Biol.* **227**, 156-168.

Sedmera, D., Pexieder, T., Rychterova, V., Hu, N. and Clark, E. B. (1999). Remodeling of chick embryonic ventricular myoarchitecture under experimentally changed loading conditions. *Anat. Rec.* **254**, 238-252.

Sedmera, D., Hu, N., Weiss, K. M., Keller, B. B., Denslow, S. and Thompson, R. P. (2002). Cellular changes in experimental left heart hypoplasia. *Anat. Rec.* **267**, 137-145.

Sehnert, A. J., Huq, A., Weinstein, B. M., Walker, C., Fishman, M. and Stainier, D. Y. (2002). Cardiac troponin T is essential in sarcomere assembly and cardiac contractility. *Nat. Genet.* **31**, 106-110.

Seidman, J. G. and Seidman, C. (2001). The genetic basis for cardiomyopathy: from mutation identification to mechanistic paradigms. *Cell* **104**, 557-567.

Shimoda, N., Knapik, E. W., Ziniti, J., Sim, C., Yamada, E., Kaplan, S., Jackson, D., de Sauvage, F., Jacob, H. and Fishman, M. C. (1999). Zebrafish genetic map with 2000 microsatellite markers. *Genomics* **58**, 219-232.

Small, E. M. and Krieg, P. A. (2000). Expression of atrial natriuretic factor (ANF) during Xenopus cardiac development. *Dev. Genes Evol.* **210**, 638-640.

Srivastava, D., Thomas, T., Lin, Q., Kirby, M. L., Brown, D. and Olson, E. N. (1997). Regulation of cardiac mesodermal and neural crest development by the bHLH transcription factor, dHAND. *Nat. Genet.* **16**, 154-160.

Stainier, D. Y. R. and Fishman, M. C. (1992). Patterning the zebrafish heart tube: acquisition of anteroposterior polarity. *Dev. Biol.* **153**, 91-101.

Stainier, D. Y. R., Fouquet, B., Chen, J. N., Warren, K. S., Weinstein, B. M., Meiler, S. E., Mohideen, M. A., Neuhauss, S. C., Solnica-Krezel, L., Schier, A. F. et al. (1996). Mutations affecting the formation and function of the cardiovascular system in the zebrafish embryo. *Development* **123**, 285-292.

Summerton, J. and Weller, D. (1997). Morpholino antisense oligomers: design, preparation, and properties. *Antisense Nucleic Acid Drug Dev.* **7**, 187-195.

Wanga, J., Eckberg, W. R. and Anderson, W. A. (2001). Ultrastructural differentiation of cardiomyocytes of the zebrafish during the 8-26-somite stages. *J. Submicrosc. Cytol. Pathol.* **33**, 275-287.

Westerfield, M. (1995). *The Zebrafish Book*. Eugene, OR: University of Oregon Press.

Xu, X., Meiler, S. E., Zhong, T. P., Mohideen, M., Crossley, D. A., Burggren, W. W. and Fishman, M. C. (2002). Cardiomyopathy in zebrafish due to mutation in an alternatively spliced exon of titin. *Nat. Genet.* **30**, 205-209.

Yelon, D. and Stainier, D. Y. (1999). Patterning during organogenesis: genetic analysis of cardiac chamber formation. *Semin. Cell Dev. Biol.* **10**, 93-98.

Yelon, D., Horne, S. A. and Stainier, D. Y. (1999). Restricted expression of cardiac myosin genes reveals regulated aspects of heart tube assembly in zebrafish. *Dev. Biol.* **214**, 23-37.

Yelon, D., Ticho, B., Halpern, M. E., Ruvinsky, I., Ho, R. K., Silver, L. M. and Stainier, D. Y. R. (2000). The bHLH transcription factor Hand2 plays parallel roles in zebrafish heart and pectoral fin development. *Development* **127**, 2573-2582.

Zeller, R., Bloch, K. D., Williams, B. S., Arceci, R. J. and Seidman, C. E. (1987). Localized expression of the atrial natriuretic factor gene during cardiac embryogenesis. *Genes Dev.* **1**, 693-698.